Inorganic Chemistry

Article

pubs.acs.org/IC

# A Binuclear $Mn^{III}$ Complex of a Scorpiand-Like Ligand Displaying a Single Unsupported $Mn^{III}$–O–$Mn^{III}$ Bridge

Salvador Blasco,*[,†] Joan Cano,[†,⊥] M. Paz Clares,[†] Santiago García-Granda,[‡] Antonio Doménech,[§] Hermas R. Jiménez,[∥] Begoña Verdejo,[†] Francesc Lloret,*[,†] and Enrique García-España*[,†]

[†]Instituto de Ciencia Molecular, Departamento de Química Inorgánica, Universidad de Valencia, C/Catedrático José Beltrán Martínez, 2, 46980, Paterna, Valencia, Spain

[‡]Departamento de Química Física y Analítica, Universidad de Oviedo, C/Julián Clavería, 8, 33006, Oviedo, Spain

[§]Departamento de Química Analítica, Universidad de Valencia, C/Dr. Moliner 50, 46100, Burjassot, Valencia, Spain

[∥]Departamento de Química Inorgánica, Universidad de Valencia, C/Dr. Moliner 50, 46100, Burjassot, Valencia, Spain

[⊥]Fundació General de la Universitat de València (FGUV), Universitat de València, E-46980 Paterna, València, Spain

Supporting Information

**ABSTRACT:** The crystal structure of a binuclear $Mn^{III}$ complex of a scorpiand-like ligand (**L**) displays an unsupported single oxo bridging ligand with a $Mn^{III}$–O–$Mn^{III}$ angle of 174.7°. Magnetic susceptibility measurements indicate strong antiferromagnetic coupling between the two metal centers. DFT calculations have been carried out to understand the magnetic behavior and to analyze the nature of the observed Jahn–Teller distortion. Paramagnetic $^1$H NMR has been applied to rationalize the formation and magnetic features of the complexes formed in solution.

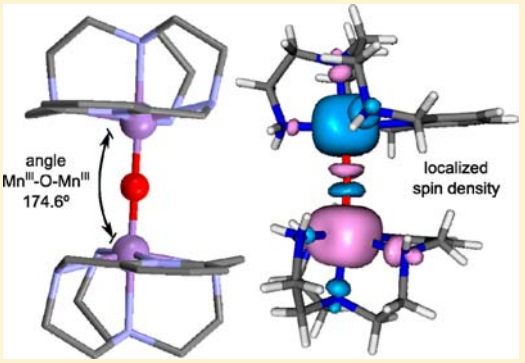


## INTRODUCTION

Manganese is an element of biological, chemical, and pharmaceutical relevance. Living systems use this essential element for important functions dealing with redox reactions such as water splitting in photosynthesis[1] or reactive oxygen species removal,[2] among others. Although many manganese enzymes such as superoxide dismutase or manganese oxygenase contain a single manganese atom[3] in their active center, a growing number of manganese enzymes with binuclear metal sites[4] such as catalases,[5,6] ribonucleotide reductase,[7] or arginase[8] are being discovered. In all these metalloenzymes, manganese is cycling between different oxidation states.

$Mn^{III}$ unsaturated polynuclear complexes have a strong tendency to form bridges between two neighboring metal atoms. The most common bridging ligand types are acetate, carbonate, water, hydroxo, and oxo anions.[6,9−13] However, the participation of a single unsupported oxo bridge ligand is rather unusual. Indeed, the formation of linear $\mu$-oxo complexes requires of a particular steric hindrance for preventing the bending of the angle or the formation of multibridged complexes.[6,9−11,13−18] Since $Mn^{III}$ is a paramagnetic atom, such binuclear complexes may exhibit interesting magnetic properties like super-antiferromagnetic behavior.[19]

Scorpiand-like ligands have a structure consisting of a macrocyclic core and a flexible pending arm containing additional donor atoms. Compound **L**, depicted in Scheme 1, which belongs to this class of ligands, is the result of the condensation of 2,6-*bis*(bromomethyl)pyridine with *tris*(aminoethyl)amine.[20] In this paper, we report that the interaction of **L** with a $Mn^{II}$ salt followed by atmospheric oxidation leads to the formation of a binuclear complex in which two $[Mn^{III}L]^{3+}$ subunits are interconnected by a single, almost linear oxo bridge, which has been studied by a variety of experimental techniques both in solution and in the solid state.

**Scheme 1. L Drawing**

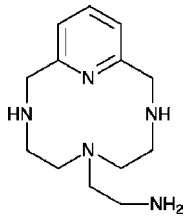


## EXPERIMENTAL SECTION

**Synthesis and Chemicals Used.** The synthetic procedure for the obtention of **L** has been already described.[20] The $Mn^{II}$ source was a

Received: July 23, 2012
Published: October 8, 2012

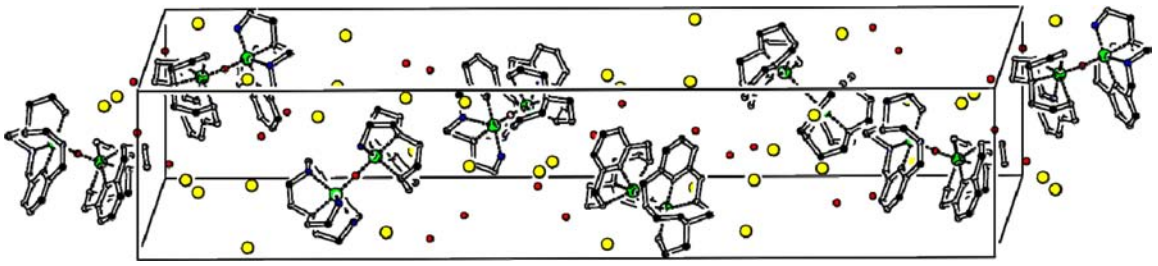

**Figure 1.** Unit cell showing the arrangement around the $6_1$ screw axis. $Br^-$ atoms, shown in yellow; water molecules, shown in red; hydrogen atoms, not displayed.

$MnSO_4 \cdot H_2O$ standardized stock solution. All other chemicals were purchased from several commercial sources and used as received.

The formation of the $[Mn_2OL_2]^{4+}$ complex is achieved by dissolving in water equivalent amounts of $L \cdot 4HBr \cdot 2H_2O$ and $Mn^{II}$ and increasing the pH up to *ca.* 7 with diluted NaOH. The formation and further oxidation of the complex can be followed by a change in the color of the solution from colorless to purple.

**X-Ray Structures.** A solution containing one equivalent of both $L \cdot 4HBr \cdot 2H_2O$ and $MnSO_4 \cdot H_2O$ at neutral pH was left to slowly evaporate in an open vessel. After several days, hexagonal dark magenta crystals suitable for X-ray diffraction were obtained.

The single crystal X-ray diffraction studies were carried out using Agilent Gemini equipment with Mo K$\alpha$ monochromatic radiation ($\lambda$ = 0.71073 Å) and a CCD detector at room temperature. The data reduction and scaling were made with the CrysAlisPro suite software.[21] The structure was solved and refined with SHELXS97 and SHELXL97, respectively.[22] The crystallographic data are collected in Table S1 (Supporting Information).

**Magnetic Measurements.** Magnetic susceptibility measurements on polycrystalline samples of compound $[Mn_2OL_2] \cdot 4Br \cdot 4H_2O$ were carried out in the 1.9−300.0 K temperature range with a Quantum Design SQUID magnetometer under an applied magnetic field of 5000 G. Corrections for the diamagnetic contribution of the constituent atoms and for the magnetization of the sample holder were applied to the raw data.

**Theoretical Computations.** Calculations were performed with the *Gaussian 09* package using the B3LYP functional and the quadratic convergence approach.[23] Triple-$\xi$ and double-$\xi$ all electron basis sets, as proposed by Ahlrichs et al., were used for the metal ions and the rest of atoms, respectively.[24] The broken symmetry approach was employed to describe the unrestricted solutions of the antiferromagnetic spin states,[25] which were obtained from the guess functions generated with the fragment tool implemented in the Gaussian code. The full geometry was used for $[Mn_2OL_2]^{4+}$. We also used a polarizable continuum model with the parameters corresponding to the acetonitrile solvent.[26] However, since similar results for the magnetic coupling constant $J$ were found, these data have not been included in the discussion. A study on molecular models was done to verify our results, to know which magnetic orbitals are responsible for the strong observed magnetic coupling and which is the most stable arrangement of the Jahn−Teller axis. These molecular models are simple, being constituted only by two $Mn^{III}$ ions, one oxo group preserving the linearity of the Mn−O−Mn axis, and ammonia groups to complete the ideal octahedral metal coordination sphere (N−Mn−N = 90°). The broken-symmetry methodology allows the determination of all the exchange coupling constants present in a polynuclear transition metal complex.[25] Since our system contains only two $Mn^{III}$ ($S$ = 2) paramagnetic centers, the magnetic coupling constant in $[Mn_2OL_2]^{4+}$ can be inferred from the energies of a nonet and a singlet spin function, displaying a parallel and antiparallel alignment of the local spin moments. The electronic spectra in acetonitrile and water solutions have been partially calculated using the time dependent formalism applied to the density functional theory (DFT).[27] In both solvents, the obtained results are similar. The inclusion of the solvent in the electronic calculations was done by using a PCM model with parameters corresponding to both acetonitrile and water.[28]

**Paramagnetic NMR Measurements.** The paramagnetic NMR measurements were acquired on a Bruker Avance 400 spectrometer operating at 399.91 MHz. One-dimensional spectra were recorded in $D_2O$ solvent with presaturation of the $H_2O$ signal during part of the relaxation delay to eliminate the $H_2O$ signal. A relaxation delay time of 200 ms, a 75 kHz spectral width, and an acquisition time of 200 ms were used. 1D spectra were processed using exponential line-broadening weighting functions as apodization with a value of 60 Hz. Chemical shifts were referenced to residual solvent protons of $D_2O$ resonating at 4.76 ppm (298 K) relative to TMS. The concentration of the samples for paramagnetic $^1H$ NMR was 5 mmol·dm$^{-3}$. The longitudinal relaxation times of the hyperfine shifted resonances were determined using the inversion recovery pulse sequence ($d_1$−180°−$\tau$−90°−$acq$, where $d_1$ is the relaxation delay and $acq$ is the acquisition time); 14 values of $\tau$ were selected between 0.8 and 500 ms.[29] ($d_1$ + $acq$) values were at least 5 times the longest expected $T_1$ ranging from 200 to 300 ms, and the number of scans was 9000. The $T_1$ values were calculated from the inversion−recovery equation. Transversal relaxation times were obtained measuring the line broadening of the isotropically shifted signals at half-height through the equation $T_2^{-1} = \pi \Delta\nu_{1/2}$.

**Electrochemical Measurements.** The electrochemistry of the monomer systems was studied in water using 0.15 M $NaClO_4$ as a supporting electrolyte. The electrochemical behavior was recorded in the 4.0−9.0 pH range under an argon atmosphere. A glassy carbon electrode was used as a working electrode, a platinum wire as an auxiliary, and Ag/AgCl as a reference electrode in a three-electrode cell coupled to a CH 420I potentiostat.

The sample was prepared by direct mixing of the ligand as hydrobromide salt and one equivalent of $MnSO_4 \cdot H_2O$ in 0.15 M of $NaClO_4$. The pH was adjusted with either $HClO_4$ or NaOH aqueous solutions.

Experiments on solutions of $[Mn_2OL_2] \cdot 4Br \cdot 4H_2O$ in 0.10 M $Bu_4NPF_6$/DMSO and 0.10 M $Bu_4NPF_6$/MeCN were performed using a Pt disk pseudoreference electrode, the potentials being measured relative to the ferrocenium/ferrocene couple using a 0.50 mM ferrocene (Fluka) internal standard.

**Spectroscopic Measurements.** UV−vis spectra were recorded in an Agilent 8453 spectrometer.

## RESULTS AND DISCUSSION

**Description of Crystal Structure of $[Mn_2OL_2] \cdot 4Br \cdot 4H_2O$.** The crystal system is hexagonal, and the unit cell contains six $[LMn−O−MnL]^{4+}$ units helicoidally arranged according to a $6_1$ screw axis (Figure 1). The $c$ axis is unusually long, 55 Å, showing long-range organization of anions and water molecules in the crystal structure. Four bromide anions and four lattice water molecules complete the structure forming the hydrogen bond network.

Each $Mn^{III}$ in a $[Mn_2OL_2]^{4+}$ moiety is coordinated in a distorted octahedral geometry (Figure 2). The pyridine nitrogen, the primary amino group of the tail, the tertiary nitrogen, and the bridging oxo group define the equatorial plane (Table 1), while the distorted axial positions are occupied


dx.doi.org/10.1021/ic3016063 | *Inorg. Chem.* 2012, 51, 11698−11706

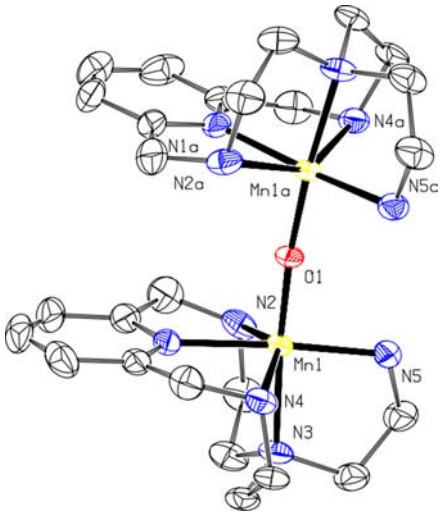


**Figure 2.** ORTEP plot for the structure $[Mn_2OL_2]^{4+}$. Bromide and water moieties and hydrogen atoms are not displayed. Thermal ellipsoids are plotted at the 50% probability level.

**Table 1. Selected Bond Lengths and Angles**

| bond length/Å | | angles/deg | |
|---|---|---|---|
| Mn1−O1 | 1.753(2) | Mn1−O1−Mn1 | 174.7(3) |
| Mn1−N2 | 2.308(4) | O1−Mn1−N5 | 93.1(2) |
| Mn1−N1 | 2.088(4) | O1−Mn1−N1 | 92.8(2) |
| Mn1−N3 | 2.101(4) | N5−Mn1−N3 | 83.3(2) |
| Mn1−N4 | 2.268(4) | N1−Mn1−N3 | 91.0(2) |
| Mn1−N5 | 2.034(4) | O1−Mn1−N4 | 97.3(1) |
| | | N5−Mn1−N4 | 107.1(2) |
| | | N1−Mn1−N4 | 77.0(2) |
| | | N3−Mn1−N4 | 81.0(2) |
| | | O1−Mn1−N2 | 102.6(1) |
| | | N5−Mn1−N2 | 97.8(2) |
| | | N1−Mn1−N2 | 76.1(2) |
| | | N3−Mn1−N2 | 80.90(2) |

by the nitrogen atoms of the two secondary amino groups close to the pyridine aromatic spacer (Mn1−N2 = 2.269(3)Å, Mn1−N4 = 2.304(6)Å; Table 1). As such an orientation of the elongation axis was already observed for related $Cu^{II}$ complexes,[20] the direction of the distortion should be somehow imposed by the ligand topology. The oxo bridge is almost linear (Mn1−O1−Mn1 = 174.7(3)°). This value agrees with the angles reported for the other few cases in which single $Mn^{III}$−O−$Mn^{III}$ bridges have been described.[10,14,16,17c,18] Steric congestion was put forward to explain a more acute angle of 146.15° reported in one of the examples.[17c] Evidence for the oxo bridge is provided by the infrared spectrum (Figure S1, Supporting Information) in which two characteristic peaks of metal−oxo−metal bonds can be found at around 870 $cm^{-1}$.[30]

The $Mn^{III}$**L** subunits are not placed one above the other but rotated 38.18° around the Mn1−O1−Mn1 axis. Moreover, both pyridine rings are not strictly parallel to each other, with an angle of 8.08° between their mean planes.

**Electronic Spectrum.** The UV−vis spectrum displayed in Figure 3 shows that, as it was reported for a related system,[14] practically there is not absorbance above 500 nm. A summary of the energy and nature of the main low-energy bands obtained in a preliminary theoretical study is displayed in Table S2 (Supporting Information). The study was done on the electronic spectrum of the *broken-symmetry* singlet by means of the *time dependent* formalism applied to DFT. The molecular orbitals involved in the electronic transitions associated with the low-energy bands are depicted in Figure 4. The theoretical calculation indicates that around 500 nm appear several very weak bands corresponding to d−d transitions in the $Mn^{III}$ ions. Such bands are observed in the experimental spectrum at around 520 nm. A more intense band is postulated at 470 nm that involves a d−d transition and a charge transfer from the $\pi$ electronic density on the pyridine group to a d metal orbital (LMCT). The last transition is the cause of the higher intensity. This transition probably corresponds to the band observed at 420 nm in the experimental spectrum. At higher energies, very intense bands are observed that can be associated with $\pi-\pi^*$

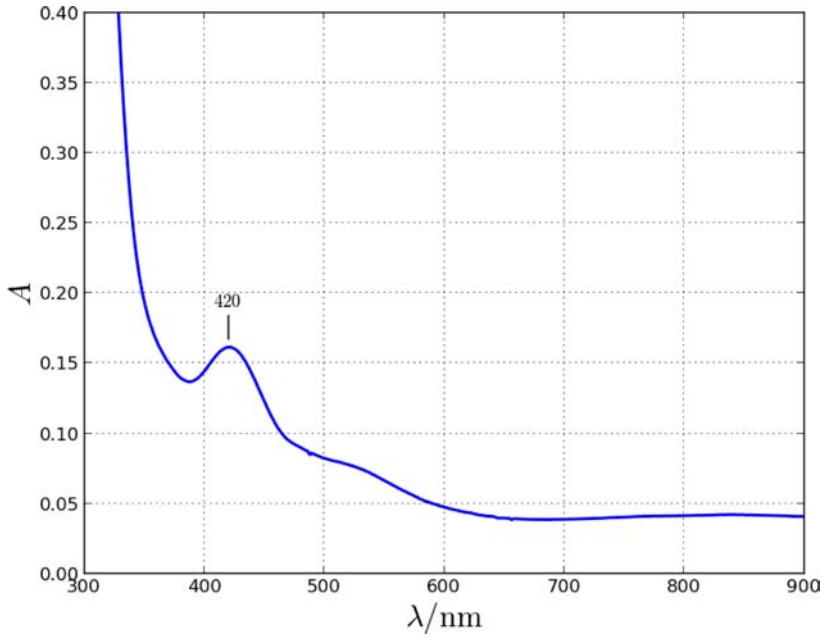


**Figure 3.** Electronic spectrum of $[Mn_2OL_2]\cdot 4Br\cdot 4H_2O$ in water.


dx.doi.org/10.1021/ic3016063 | *Inorg. Chem.* 2012, 51, 11698−11706

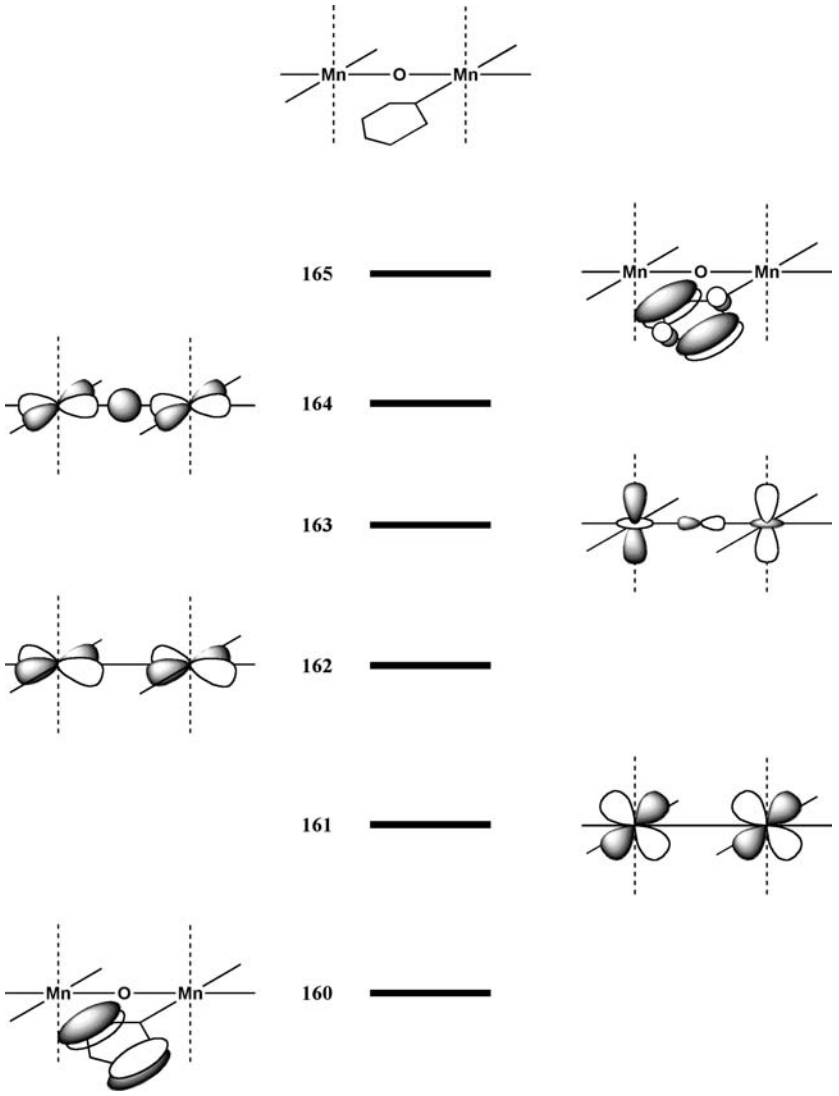


**Figure 4.** Main selected molecular orbitals involved in the electronic transitions shown in Table S2 (Supporting Information).

transitions in the ligand. These intense bands hide other less intense electronic transitions such as those of moderate intensity that, as predicted by the theoretical study, should appear at 365 and 325 nm. These bands can be attributed to a mixture between metal−metal (MM'CT) and metal−ligand (MLCT) charge transfers.

**Magnetic Properties.** The molar magnetic susceptibility, $\chi_M$, for $[Mn_2OL_2]\cdot 4Br\cdot 4H_2O$ was measured on grounded crystals as a function of the temperature, $T$. The results are shown in Figure 5 in the form of a $\chi_M T$ *versus* $T$ plot. At room temperature, the value of $\chi_M T$ of 0.65 $cm^3\ mol^{-1}\ K$ is very much lower than that expected for two magnetically non-interacting high-spin $Mn^{III}$ ions [$\chi_M T = (2N\beta^2 g^2/3k)S(S+1) = 6.0\ cm^3\ mol^{-1}\ K$ for $S = 2$ and $g = 2$]. Upon cooling, $\chi_M T$ continuously decreases, and it vanishes below 50 K. This behavior is characteristic of a strong antiferromagnetic coupling between two $S = 2$ spins. The data were fitted by the theoretical expression derived from an isotropic spin exchange Hamiltonian $H = -JS_1S_2$ [eq 1].

$$\chi_M = \frac{2N\beta^2 g^2}{kT}\,\frac{e^x + 5e^{3x} + 14e^{6x} + 30e^{10x}}{1 + 3e^x + 5e^{3x} + 7e^{6x} + 9e^{10x}} \qquad (1)$$

with $x = J/kT$.

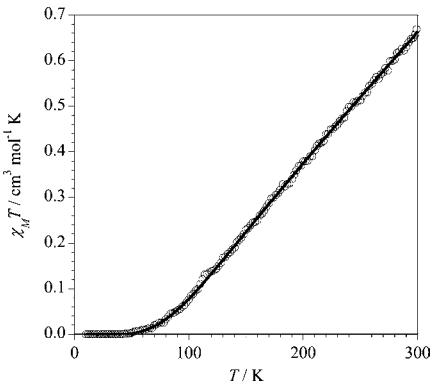


**Figure 5.** Temperature dependence of $\chi_M T$ for $[Mn_2OL_2]\cdot 4Br\cdot 4H_2O$. The solid line is the best fit (see text).

The best fit was obtained with $g = 2$ (kept constant) and $J = -249(2)\ cm^{-1}$. Both the magnitude and sign of the $J$ value are comparable to those observed for other quasi-linear $Mn^{III}-O-Mn^{III}$ cores.[14,15]

However, since, as above stated, there are very few examples of $Mn^{III}$ dinuclear comples with only one oxo bridging ligand, a magneto-structural correlation cannot be established.[10,14,17c]


dx.doi.org/10.1021/ic3016063 | *Inorg. Chem.* 2012, 51, 11698−11706

Moreover, unexpected weak antiferromagnetic coupling has been reported in two cases. In the other cases, the values of the $Mn^{III}-O-Mn^{III}$ angle fall in a small range close to linearity (−168.5 to 180°), and there is not a clear-cut correlation with the antiferromagnetic coupling constants ($J$ from −165.9 to −251.2 $cm^{-1}$). Nevertheless, a discussion about the superexchange pathway in this compound is given below.

**Theoretical Computations.** DFT calculations of the experimental geometry of complex $[Mn_2OL_2]^{4+}$ were performed in order to estimate the magnetic coupling constant between the two $Mn^{III}$ centers. The obtained $J$ value of −244.1 $cm^{-1}$ supports a strong antiferromagnetic nature for the coupling. A detailed analysis of the molecular geometry of $[Mn_2OL_2]^{4+}$ shows that the $Mn^{III}$ ions have, because of a second order Jahn−Teller effect, an elongation in an axis noted as the Jahn−Teller axis. Thus, the electronic configuration of the high-spin $Mn^{III}$, $3d^4$, involves the three $t_{2g}$ orbitals and the $d_{z^2}$ orbitals. Only these orbitals, not all of them, act as magnetic orbitals and contribute to the magnetic coupling. Since the $d_{z^2}$ orbital delocalizes in the $\sigma$ pathway, it is usually thought that this orbital is mainly responsible for the strong antiferromagnetic coupling. However, the Jahn−Teller axis is placed perpendicular to the exchange pathway direction. Thus, only the electronic density of the $d_{z^2}$ ring, and not the larger electronic density on the axial lobe, will be delocalized on the exchange pathway. This situation should not favor a large magnetic coupling. However, the exchange pathway is short enough to magnify the magnetic coupling, and moreover, the contribution from the $t_{2g}$ orbitals to magnetic coupling can be significant. A search in the Cambridge Database shows that, even if only a few examples are reported of $Mn^{III}$ binuclear systems with a single oxo group acting as bridging ligand between the metal ions, in all of them an elongated or compressed Jahn−Teller axis is aligned perpendicular[6,9] or parallel[9,10,14,15,17] to the linear or quasi-linear $Mn^{III}-O-Mn^{III}$ exchange pathway, respectively (models A and D in Figure 4), the latter case being the most usual. There is also a case with an octahedral-like geometry and another one with a square pyramidal coordination sphere where exceptionally the $Mn^{III}-O-Mn^{III}$ angle is far from linearity.[12,16] In those systems in which magnetic measurements were performed, a strong antiferromagnetic coupling was observed.[10,14,15] In order to understand the preference for this arrangement and the qualitative contribution of each magnetic orbital, we have performed electronic calculations on simplified binuclear models built up as explained in the caption to Figure 6.

The Mn−N(ammonia) and Mn−O bond lengths have been optimized forcing axial elongation and compression for different Jahn−Teller orientations (see Figure 6). In agreement with the experimental data, the most stable conformation is that showing a compression in a Jahn−Teller axis that involves the Mn−O bond (conformation D). However, conformation A with an axial elongation perpendicular to the Mn−O axis, observed in $[Mn_2OL_2]^{4+}$ and also in some complexes of the literature, is just at 0.75 kcal/mol. Hence, both conformations can be found, and only the adequate design of the peripheral ligand benefits one of them. Since in our models there are not restrictions in peripheral ligands, conformation B (contraction in a perpendicular direction to the Mn−O axis) converges to the most stable conformation A. Finally, model C, where axial elongation is placed on the Mn−O axis, is clearly unstable (26.75 kcal/mol). These results allow for an explanation of the observation of two preferential conformations in the literature.

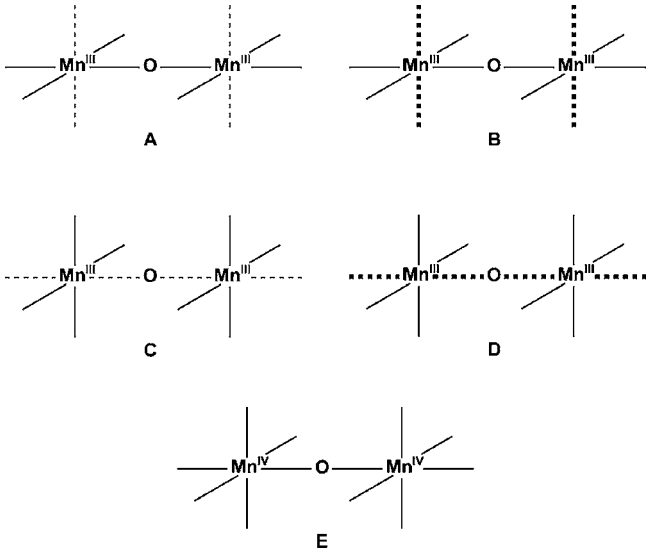


**Figure 6.** Molecular models used in the DFT study. Thin and thick dotted lines are employed for elongated and compressed Jahn−Teller axes, repectively. The oxidation state of the metal ion is indicated as a superscript character.

In the two most stable conformations (A and D), strong antiferromagnetic coupling is expected (−143.3 and −163.4 $cm^{-1}$, respectively) but moderately stronger in the last case. It makes sense if we bear in mind that the electronic delocalization from the magnetic orbitals to the pathway is larger for shorter Mn−O bond lengths and that this electronic promotion is larger for $d_{z^2}$ than for $d_{x^2-y^2}$. While the electronic density on the equatorial ring lobe of the $d_{z^2}$ is pointing to the Mn−O axis, the $d_{x^2-y^2}$ orbital does not overlap with the oxo orbitals. On the other hand, a similar model has been built for $Mn^{IV}$ ions, E, where only the $t_{2g}$ orbitals acts as magnetic orbitals. Also, a strong antiferromagnetic coupling is found ($J$ = −112.3 $cm^{-1}$). Even though, to our knowledge, there are not any experimental data for such systems, the obtained result is supported by those obtained for mixed $Mn^{III}-Mn^{IV}$ $\mu$-oxo complexes that also present strong antiferromagnetic coupling.[14] In the last cases, the magnetic coupling is stronger probably because it can be associated with partial charge transfers assisted by the mixed valence character and the nature of the peripheral ligands.[11] In any case, to compare qualitatively the contribution to the magnetic coupling of the $t_{2g}$ and $e_g$ orbitals, we must use the $n^2J$ product, where $n$ is the number of unpaired electrons per center. Notwithstanding that this procedure is purely qualitative because some metal−ligand distances have been modified, it can be intuitive and useful. This product takes the absolute values 2293, 2614, and 1011 for A, D, and E, respectively. The large value for E proves that the contribution of $t_{2g}$ orbitals is important, as it was suggested and indirectly well proved by Girerd et al.[11,14] However, the large difference between this value and that for modes A and D supports that the contribution of the $d_{z^2}$ orbital is also important.

**Paramagnetic NMR Measurements.** Paramagnetic $^1H$ NMR spectroscopy is a powerful technique for evaluating the coordination geometry and electronic structure of metal complexes in solution.[31−33] Usually, mono- and binuclear $Mn^{III}$ have short electronic relaxation times and, thus, are expected to present well resolved isotropically shifted $^1H$ NMR spectra.[31] The isotropic shifts of proton resonances in


dx.doi.org/10.1021/ic3016063 | Inorg. Chem. 2012, 51, 11698−11706

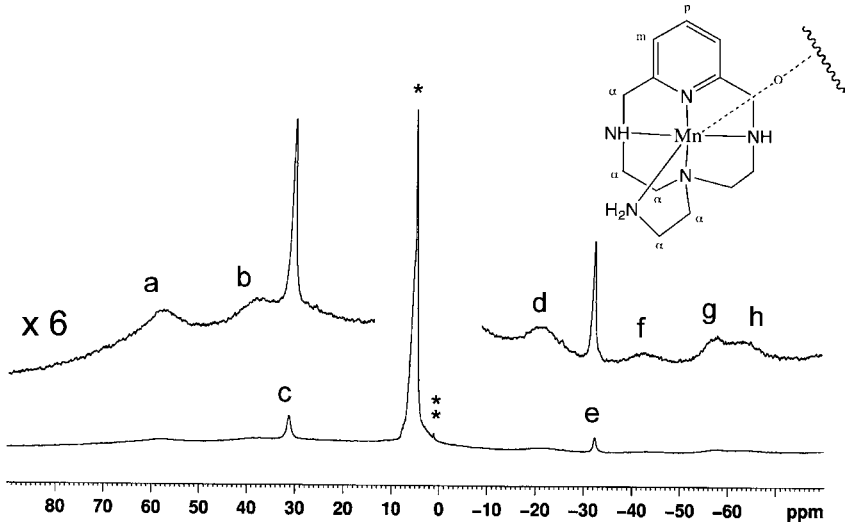


**Figure 7.** 400 MHz proton NMR spectra in $D_2O$ at pD = 7 and 298 K of $[Mn_2OL_2]\cdot 4Br\cdot H_2O$ 5 mM. The asterisks mark the residual solvents (*, $H_2O$; **, HOD).

**Table 2. $^1$H NMR Hyperfine-Shifted Resonances of $[Mn_2OL_2]$ Complex in $D_2O$ at 298 K and pD 7**

| signal | $\delta$ (ppm) | no. of protons | assignments | temperature dependence | $T_1$ (ms) | $\Delta\nu_{1/2}$ (Hz) | $T_2{}^a$ (ms) |
|---|---|---|---|---|---|---|---|
| a | 57.4 | | | Curie | <1 | 2210 | 0.14 |
| b | 38.0 | | | Curie | <1 | 1360 | 0.23 |
| d | −21.3 | | | Curie | <1 | 2260 | 0.14 |
| f | −42.9 | 32 | $\alpha CH_2$ | Curie | <1 | 2260 | 0.14 |
| g | −57.4 | | | Curie | <1 | *b* | *b* |
| h | −63.0 | | | Curie | <1 | *b* | *b* |
| c | 31.3 | 4 | $H_m$−py | Curie | ∼1.2 | 290 | 1.1 |
| e | −32.2 | 2 | $H_p$−py | Curie | ∼1.5 | 240 | 1.3 |

[a]Measured from the linewidth at half-height. [b]Overlap prevents measurement of this value.

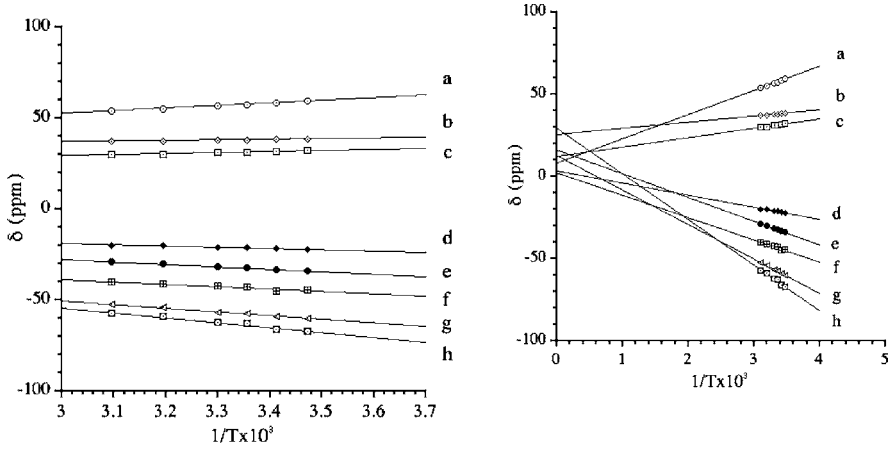


**Figure 8.** Temperature dependence of the $^1$H NMR isotropic shifts of the $[Mn_2OL_2]^{4+}$ complex at pD = 7. Temperature range 288−323 K.

paramagnetic systems may be of contact or dipolar origin or a combination of both, $(\Delta H/H_0)^{iso} = (\Delta H/H_0)^{con} + (\Delta H/H_0)^{dip}$. As already described in the literature,[34,36] high-spin $Mn^{III}$ and binuclear $Mn^{III}$ complexes have large contributions by contact shift.[35,36]

In this work, we have studied the electronic properties of the $[Mn_2OL_2]\cdot 4Br\cdot 4H_2O$ complex dissolved in water. We have recorded the paramagnetic $^1$H NMR spectra, measured the $^1$H longitudinal and transversal relaxation times, $T_1$ and $T_2$, and analyzed the temperature dependence of the chemical shifts.

The $^1$H NMR spectrum of the binuclear $[Mn_2OL_2]^{4+}$ complex cation recorded in $D_2O$ at pD = 7 shows, in the downfield region, three well resolved isotropically shifted signals (a−c; see Figure 7). In addition, it displays five upfield shifted signals (d−h). Hyperfine-shifted resonances, linewidths at half-height, and longitudinal relaxation time values ($T_1$) are reported in Table 2. The isotropically shifted signals show linewidths, measured at half-height, of around 1300−2200 Hz, except signals c and e with linewidths of 290 and 240 Hz, respectively. Longitudinal relaxation times vary from less than 1 ms to ∼1.5 ms for signal e. $T_1$ measurements along with the


dx.doi.org/10.1021/ic3016063 | *Inorg. Chem.* 2012, 51, 11698−11706

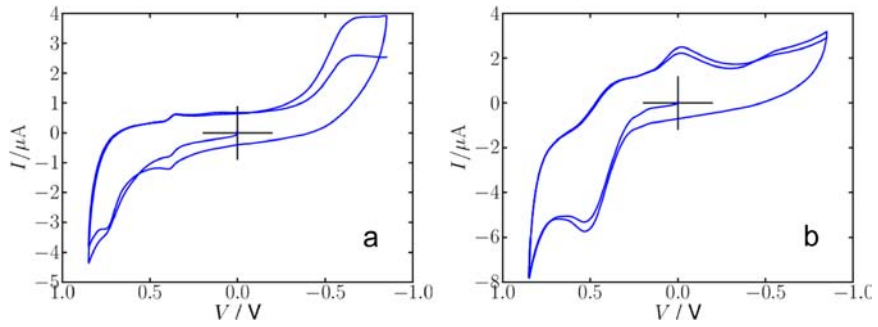


**Figure 9.** Cyclic voltammograms at a glassy carbon electrode for a 1.0 mM Mn/**L** solution in 0.15 M $NaClO_4$ at pH 3.0 (a) and 7.0 (b). Potential scan rate 50 mV/s.

observed chemical shift values and $\Delta\nu_{1/2}$ are characteristic of binuclear $Mn^{III}$ complexes.[34,36] The group of signals a, b, d, and f–h, integrates 32 protons and can be assigned on the basis of the extremely short $T_1$ values and large chemical shifts to the $CH_2$ protons closest to the manganese centers in $Mn^{III}_2O\mathbf{L}_2$ ($\alpha$-$CH_2$, see inset in Figure 7). As described in the literature,[36] $\alpha$-$CH_2$ protons in spin-coupled $Mn^{III}$ complexes have similar large shifts, broad linewidths, and short $T_1$ values. The other group of signals (c, e), which have a longer relaxation time ($T_1$ ~1.2 and ~1.5 ms respectively) and relatively narrow signals ($\Delta\nu_{1/2}$ of 290 and 240 Hz respectively), agree with the assignment to *meta* and *para* pyridine protons, respectively (see Table 2).

The above-mentioned isotropic shift resonances in paramagnetic systems can have a contact or dipolar origin or a combination of both. The contact term presents a linear dependency with the inverse of the temperature ($T^{-1}$), whereas the dipolar term is a function of $T^{-2}$.[37] Thus, it is possible to use the dependency on the isotropic shift resonances with the temperature to estimate the relative importance of these contributions. Nevertheless, due to the fact that the studied interval of temperatures is narrow because of the limitations imposed by the solvent, typically an inversely proportional change of the isotropic shift resonances is observed with the temperature. Deviations due to a small $T^{-2}$ component cannot be detected. The extrapolation to infinite temperature in the plot of $\delta$ as a function of the $T^{-1}$ is the method used for the study of the dependency type of the isotropic shifts with the temperature. Important deviations from the zero extrapolation out of the diamagnetic region will indicate the existence of a dipolar contribution to the isotropic shifts. Variable temperature $^1H$ NMR spectra of $[Mn_2O\mathbf{L}_2]\cdot 4Br\cdot 4H_2O$ at pD = 7 were registered from 288 to 323 K. In Figure 8, the observed isotropic shift resonances are plotted as a function of $T^{-1}$. All isotropic shift resonances follow a Curie behavior as they invariably decrease with increasing temperature. The isotropic shift signals h and e are more temperature dependent and show an appreciable deviation from the zero extrapolation at 29.6 and 15.9 ppm, respectively. As described above, these results are indicative of some dipolar contribution to the hyperfine shifted resonances originated by the presence of a zero-field splitting and consequently of certain magnetic anisotropy. The other signals show $\delta$ intercept values at infinite temperature within or close to the diamagnetic region and are in general indicative of a predominant contact contribution. These results agree with the existence of a magnetically coupled binuclear $Mn^{III}$ system with antiferromagnetic coupling. The paramagnetic NMR results are consistent with the magnetic studies described and show that the $[Mn_2O\mathbf{L}_2]\cdot 4Br\cdot 4H_2O$ complex present in solution has similar electronic properties as that in the solid state.

**Electrochemistry.** Figure 9 collects cyclic voltamperograms of aqueous solutions of $Mn^{II}$ and **L** recorded at pH < 6. The electrochemical response is essentially identical to that of uncomplexed $Mn^{II}$ solutions, consisting of an irreversible oxidation signal at +0.70 V vs Ag/AgCl, corresponding to the oxidation of the free $Mn^{II}$ to $MnO_2$,[38] preceded by a weak reversible wave at a midpeak potential of +0.40 V attributable to one-electron oxidation of $Mn^{II}$ ions adsorbed on the electrode surface to adsorbed $Mn^{III}$ ones. In the region of negative potentials, there is a cathodic wave at −0.58 V corresponding to a two-electron reduction of $Mn^{II}$ (see Figure 9a).

Above pH = 6, the complex starts forming, and the electrochemical response changes dramatically. The couple at +0.40 V and the oxidation peak at +0.70 V disappear, while a new oxidation peak appears at +0.55 V (see Figure 9b) followed, in the subsequent cathodic scan, by weak reduction peaks at +0.44 and −0.08 V. On the basis of the variation of peak potentials with the potential scan rate and the pH, it was concluded that the oxidation process at +0.55 V corresponds to a reversible one electron transfer process followed by a rapid chemical reaction (EC mechanism),[39] possibly due to dissociation or ligand reorganization. Accordingly, cathodic peaks at +0.44 and −0.08 V correspond to the reduction of different $Mn^{III}$ species electrochemically generated.

Figure 10 shows the cyclic voltammetric response at a glassy carbon electrode of a deaerated 1.0 mM solution of $[Mn_2O\mathbf{L}_2]\cdot 4Br\cdot 4H_2O$ in 0.10 M $Bu_4NPF_6$/DMSO. In the initial anodic scan, two overlapping peaks at +0.25 ($A_1$) and +0.53 V ($A_2$) vs coupled $Fc^+$/Fc appear in the subsequent cathodic scan, with weaker reduction peaks at +0.65 ($C_2$) and +0.35 V ($C_1$). This voltammetric profile corresponds to two successive one-electron transfer processes which can be judged as nearly reversible on the basis of the anodic-to-cathodic peak potential separation, which tends to 60 mV at low potential scan rates for both couples. No initial reduction processes were detected in the investigated potential window. The observed voltammetric response can be described in terms of two successive one-electron transfer processes as

$$\text{couple } A_1/C_1: \ [Mn^{III}\mathbf{L}-O-\mathbf{L}Mn^{III}]^{4+} \rightarrow [Mn^{IV}\mathbf{L}-O-\mathbf{L}Mn^{III}]^{5+} + e^- \quad (2)$$

$$\text{couple } A_2/C_2: \ [Mn^{III}\mathbf{L}-O-\mathbf{L}Mn^{IV}]^{5+} \rightarrow [Mn^{IV}\mathbf{L}-O-\mathbf{L}Mn^{IV}]^{6+} + e^- \quad (3)$$


dx.doi.org/10.1021/ic3016063 | *Inorg. Chem.* 2012, 51, 11698–11706

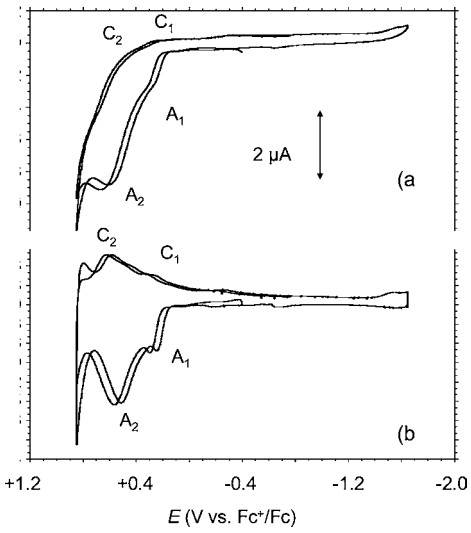


**Figure 10.** Cyclic voltammogram (a) and its deconvoluted curve (b) recorded at a glassy carbon electrode of a deaerated 1.0 mM solution of $Mn_2OL_2$ in 0.10 M $Bu_4NPF_6$/DMSO. Potential scan rate 20 mV/s.

Oxidized forms are stable on the time scale of voltammetric experiments, as denoted by the maintenance of the voltammetric pattern in repetitive voltammetry, thus suggesting that a similar $Mn^{IV}$ O-bridged complex is finally formed.

## CONCLUSIONS

The crystal structure of the binuclear $Mn^{III}$ complex $[Mn_2OL_2]\cdot 4Br\cdot 4H_2O$ exhibits a single oxo bridging ligand with a large $Mn^{III}-O-Mn^{III}$ angle. Magnetic susceptibility measurements indicate a strong antiferromagnetic coupling between the metal centers ($J = -249(2)$ $cm^{-1}$). The paramagnetic NMR studies support the same structure as well as an antiferromagnetic coupling for the binuclear complex in solution. Electrochemical data suggest that the complex is reversibly oxidized in DMSO via two successive one-electron transfer processes forming, presumably, a similar binuclear $Mn^{IV}$ complex.

## ASSOCIATED CONTENT

### Supporting Information

Crystallographic data, selected experimental and calculated electronic transition energy data, and a crystallographic information file. This material is available free of charge via the Internet at http://pubs.acs.org.

## AUTHOR INFORMATION

### Corresponding Author

*E-mail: enrique.garcia-es@uv.es, francisco.lloret@uv.es.

### Notes

The authors declare no competing financial interest.

## ACKNOWLEDGMENTS

Financial support by the Spanish Ministerio de Economía y Competitividad and FEDER funds of the E. U. (Projects CTQ2009-14288-CO4-01, CTQ2010-15364, and CONSOLIDER INGENIO 2010 CSD2010-00065 and CSD2007-00010), Generalitat Valenciana (PROMETEO 2011/008 and 2009/108) is gratefully acknowledged. B.V. wants to thank the Spanish Ministerio de Economía y Competitividad for a Juan de la Cierva Postdoctoral contract.

## REFERENCES

(1) (a) McEvoy, J. P.; Brudvig, G. W. *Chem. Rev.* **2006**, *106*, 4455–4483. (b) de Paula, J. C.; Brudvig, G. W. *J. Am. Chem. Soc.* **1985**, *107*, 2643–2648.
(2) Amy, J. W.; Penner-Hahn, J. E.; Pecoraro, V. L. *Chem. Rev.* **2004**, *104*, 903–938.
(3) Whittaker, J. W. *Metal Ions in Biological Systems*; Sigel, A., Sigel, H., Eds.; Marcel Dekker: New York, 2000.
(4) Dismukes, G. C. *Chem. Rev.* **1996**, *96*, 2909–2926.
(5) (a) Allgood, G. S.; Perry, J. J. *J. Bacteriol.* **1986**, *168*, 563–567. (b) Barynin, V. V.; Hempstead, P. D.; Vagin, A. A.; Antonyuk, S. V.; Melik-Adamyan, W. R.; Lamzin, V. S.; Harrison, P. M.; Artymiuk, P. J. *J. Inorg. Biochem.* **1997**, *67*, 196. (c) Beyer, W. F., Jr.; Fridovich, I. *Biochemistry* **1985**, *24*, 6460–6467. (e) Kono, Y.; Fridovich, I. *J. Biol. Chem.* **1983**, *258*, 6015–6019.
(6) Triller, M. U.; Hsieh, W.-Y.; Pecoraro, V. L.; Rompel, A.; Krebs, B. *Inorg. Chem.* **2002**, *41*, 5544–5554.
(7) Auling, G.; Follmann, H. *Metal Ions in Biological Systems*; Sigel, A., Sigel, H., Eds.; Marcel Dekker: New York, 1994.
(8) Ash, D. E.; Cox, J. D.; Christianson, D. W. *Metal Ions in Biological Systems*; Sigel, A., Sigel, H., Eds.; Marcel Dekker: New York, 2000.
(9) Baffert, C.; Collomb, M.-N.; Deronzier, A.; Pécaut, J.; Limburg, J.; Crabtree, R. H.; Brudvig, G. W. *Inorg. Chem.* **2002**, *41*, 1404–1411.
(10) Ghosh, K.; Eroy-Reveles, A. A.; Olmstead, M. M.; Mascharak, P. K. *Inorg. Chem.* **2005**, *44*, 8469–8475.
(11) Hotzelmann, R.; Wieghardt, K.; Flörke, U.; Haupt, H. J.; Weatherburn, D. C.; Bonvoisin, J.; Blondin, G.; Girerd, J.-J. *J. Am. Chem. Soc.* **1992**, *114*, 1681–1696.
(12) Liu, Y.; Dou, J.; Niu, M.; Zhang, X. *Acta Crystallogr.* **2007**, *E63*, m2771.
(13) Sheats, J. E.; Czernuszewicz, R. S.; Dismukes, G. C.; Rheingold, A. L.; Petrouleas, V.; Stubbe, J.; Armstrong, W. H.; Beer, R. H.; Lippard, S. J. *J. Am. Chem. Soc.* **1987**, *109*, 1435–1444.
(14) Horner, O.; Anxolabéhère-Mallart, E.; Charlot, M.-F.; Tchertanov, L.; Guilhem, J.; Mattioli, T. A.; Boussac, A.; Girerd, J.-J. *Inorg. Chem.* **1999**, *38*, 1222–1232.
(15) Kipke, C. A.; Scott, M. J.; Gohdes, J. W.; Armstrong, W. H. *Inorg. Chem.* **1990**, *29*, 2193–2194.
(16) Meng, Q.; Wang, L.; Liu, Y.; Pang, Y. *Acta Crystallogr.* **2008**, *E64*, m204.
(17) (a) Vogt, L. H., Jr.; Zalkin, A.; Templeton, D. H. *Science* **1966**, *151*, 569–570. (b) Vogt, L. H., Jr.; Zalkin, A.; Templeton, D. H. *Inorg. Chem.* **1967**, *6*, 1725–1730. (c) Coggins, M. K.; Toledo, S.; Shaffer, E.; Kaminsky, W.; Shearer, J.; Kovacs, J. A. *Inorg. Chem.* **2012**, *51*, 6633–6644.
(18) Kitajima, N.; Osawa, M.; Tanaka, M.; Morooka, Y. *J. Am. Chem. Soc.* **1991**, *113*, 8952–8953.
(19) (a) Delfs, C. D.; Stranger, R. *Inorg. Chem.* **2000**, *39*, 491–495. (b) Plaksin, P. M.; Stoufer, R. C.; Mathew, M.; Palenik, G. J. *J. Am. Chem. Soc.* **1972**, *94*, 2121–2122.
(20) Verdejo, B.; Ferrer, A.; Blasco, S.; Castillo, C. E.; González, J.; Latorre, J.; Máñez, M. A.; Basallote, M. G.; Soriano, C.; García-España, E. *Inorg. Chem.* **2007**, *46*, 5707–5719.
(21) *CrysAlisPro*, version 1.171.33.48 (release 15–09–2009 CrysAlis171 .NET); Oxford Diffraction Ltd.: England, 2009.
(22) Sheldrick, G. *Acta Crystallogr.* **2008**, *A64*, 112–122.
(23) (a) Frisch, M. J.; Trucks, G. W.; Schlegel, H. B.; Scuseria, G. E.; Robb, M. A.; Cheeseman, J. R.; Scalmani, G.; Barone, V.; Mennucci, B.; Petersson, G. A.; Nakatsuji, H.; Caricato, M.; Li, X.; Hratchian, H. P.; Izmaylov, A. F.; Bloino, J.; Zheng, G.; Sonnenberg, J. L.; Hada, M.; Ehara, M.; Toyota, K.; Fukuda, R.; Hasegawa, J.; Ishida, M.; Nakajima, T.; Honda, Y.; Kitao, O.; Nakai, H.; Vreven, T.; Montgomery, J. A., Jr.; Peralta, J. E.; Ogliaro, F.; Bearpark, M.; Heyd, J. J.; Brothers, E.; Kudin, K. N.; Staroverov, V. N.; Kobayashi, R.; Normand, J.; Raghavachari, K.; Rendell, A.; Burant, J. C.; Iyengar, S. S.; Tomasi, J.; Cossi, M.; Rega, N.; Millam, N. J.; Klene, M.; Knox, J. E.; Cross, J. B.; Bakken, V.; Adamo, C.; Jaramillo, J.; Gomperts, R.; Stratmann, R. E.; Yazyev, O.; Austin, A. J.; Cammi, R.; Pomelli, C.; Ochterski, J. W.; Martin, R. L.; Morokuma, K.; Zakrzewski, V. G.; Voth, G. A.; Salvador, P.;

Dannenberg, J. J.; Dapprich, S.; Daniels, A. D.; Farkas, Ö.; Foresman, J. B.; Ortiz, J. V.; Cioslowski, J.; Fox, D. J. *Gaussian 09*, Revision A.1; Gaussian, Inc.: Wallingford, CT, 2009. (b) Becke, A. D. *Phys. Rev. A* **1988**, *38*, 3098−3100. (c) Becke, A. D. *J. Chem. Phys.* **1993**, *98*, 5648−5652. (d) Lee, C.; Yang, W.; Parr, R. G. *Phys. Rev. B* **1988**, *37*, 785−789.

(24) (a) Schäfer, A.; Horn, H.; Ahlrichs, R. *J. Chem. Phys.* **1992**, *97*, 2571−2577. (b) Schäfer, A.; Huber, C.; Ahlrichs, R. *J. Chem. Phys.* **1994**, *100*, 5829−5835.

(25) (a) Ruiz, E.; Cano, J.; Álvarez, S.; Alemany, P. *J. Am. Chem. Soc.* **1998**, *120*, 11122−11129. (b) Ruiz, E.; Cano, J.; Álvarez, S.; Alemany, P. *J. Comput. Chem.* **1999**, *20*, 1391−1400. (c) Ruiz, E.; Llunell, M.; Cano, J.; Rabu, P.; Drillon, M.; Massobrio, C. *J. Phys. Chem. B* **2006**, *110*, 115−118. (d) Ruiz, E.; Rodríguez-Fortea, A.; Cano, J.; Álvarez, S.; Alemany, P. *J. Comput. Chem.* **2003**, *24*, 982−989.

(26) Tomasi, J.; Mennucci, B.; Cammi, R. *Chem. Rev.* **2005**, *105*, 2999−3094.

(27) Casida, M. E.; Jamorski, C.; Casida, K. C.; Salahub, D. R. *J. Chem. Phys.* **1998**, *108*, 4439−4449.

(28) (a) Cossi, M.; Rega, N.; Scalmani, G.; Barone, V. *J. Comput. Chem.* **2003**, *24*, 669−681. (b) Tomasi, J.; Mennucci, B.; Cances, E. *J. Mol. Struct.: THEOCHEM* **1999**, *464*, 211−226.

(29) Vold, R. L.; Waugh, J. S.; Klein, M. P.; Phelps, D. E. *J. Chem. Phys.* **1968**, *48*, 3831.

(30) Nakamoto, K. *Infrared and Raman Spectra of Inorganic and Coordination Compounds: Applications in Coordination, Organometallic, and Bioinorganic Chemistry*; Wiley: New York, 1999.

(31) Bertini, I.; Luchinat, C.; Parigi, G. *Solution NMR of Paramagnetic Molecules, Vol. 2: Applications to Metallobiomolecules and Models (Current Methods in Inorganic Chemistry)*; Elsevier: Amsterdam, 2001.

(32) Bertini, I.; Luchinat, C.; Parigi, G. *Adv. Inorg. Chem.* **2005**, *57*, 105.

(33) Kadish, K. M.; Smith, K. M.; Guilard, R. *The Porphyrin Handbook*; Academic Press: San Diego, CA, 2000.

(34) Palopoli, C.; Gonzalez-Sierra, M.; Robles, G.; Dahan, F.; Tuchagues, J. P.; Signorella, S. *J. Chem. Soc., Dalton Trans.* **2002**, 3813−3819.

(35) Wu, F. J., Jr.; Kurtz, D. M.; Hagen, K. S.; Nyman, P. D.; Debrunner, P. G.; Vankai, V. A. *Inorg. Chem.* **1990**, *29*, 5174−5183.

(36) Hage, R.; Gunnewegh, E. A.; Niël, J.; Tjan, F. S. B.; Weyhermüller, T.; Wieghardt, K. *Inorg. Chim. Acta* **1998**, *268*, 43−48.

(37) La Mar, G. N.; Horrocks, W. D.; Holm, R. H. *NMR of Paramagnetic Molecules: Principles and Applications*; Academic Press: New York, 1973.

(38) (a) Bodoardo, S.; Brenet, J.; Maja, M.; Spinelli, P. *Electrochim. Acta* **1994**, *39*, 1999−2004. (b) Rodrigues, S.; Shukla, A. K.; Munichandraiah, N. *J. Appl. Electrochem.* **1998**, *28*, 1235−1241.

(39) Nicholson, R. S.; Shain, I. *Anal. Chem.* **1964**, *36*, 706−723.